JOURNAL OF MATERIALS SCIENCE 18 (1983) 1836–1844

Fatigue crack advance mechanisms in polymers: rubber toughening mechanisms in blends of poly(2,6-dimethyl-1,4-phenylene oxide) and polystyrene

T. A. MORELLI, M. T. TAKEMORI
Polymer Physics and Engineering Branch, Corporate Research and Development, General Electric Company, Schenectady, New York 12301, USA

The fatigue crack propagation behaviour of rubber toughened blends of poly(2,6-dimethyl–1,4-phenylene oxide) (PXE) and polystyrene (PS) were studied. The nature of the fatigue crack tip damage zone development and the subsequent crack tip advance mechanism through this damage zone were also examined. In the control blend with no rubber particles, several long crazes preceded the crack tip and provided an easy path for crack propagation. The addition of rubber particles, however, led to massive microcrazing over a considerably enlarged zone about the crack tip. This proved to be an effective energy dissipation mechanism which resulted in reduced fatigue crack growth rates. When PS was substituted for PXE in the polymer matrix, although microcrazing still occurred over an enlarged crack tip damage zone, many of the microcrazes grew to macroscopic size, thus reducing the fatigue toughness.

1. Introduction

The toughening mechanism in rubber modified polymer systems has been extensively studied under static or monotonic loading conditions (see, e.g. [1, 2]). In these studies, it was found that fracture resistance was increased by introducing energy absorbing mechanisms. As a result, two basic approaches to fracture toughness have been developed: 1. the addition of an elastomeric or rubbery phase to initate massive crazing, and 2. the selective blending or chemical modification of the polymer matrix to promote extensive shear flow and to increase craze growth resistance.

Bucknall *et al.* [3] have confirmed experimentally both of these toughening mechanisms in creep studies on blends of poly(2,6-dimethyl–1,4-phenylene oxide) (PXE) and high impact polystyrene (HIPS). They concluded that massive crazing and shear band formation were responsible for the large energy dissipation in the toughening of these blends. More recently, Maxwell and Yee [4] used similar blends of PXE and HIPS in tensile tests at different strain rates and observed that the higher content PXE blends developed many short crazes and extensive shear banding, which led to greater overall ductility and toughness.

The fracture resistance of rubber toughened polymers under cyclic loading, however, has not been so extensively studied. In lifetime studies on polystyrene (PS) and HIPS, Sauer and co-workers [5, 6] observed a decrease in fatigue resistance in the rubber toughened HIPS, which was attributed to the reduced times for craze initiation due to stress concentration about the rubber particles. Other studies by Bucknall and Stevens [7] showed that the dominant damage mechanisms responsible for cyclic softening was crazing in HIPS and shear yielding in acrylonitrile–butadiene–styrene polymer (ABS). In fatigue crack propagation (FCP) studies by Hertzberg, Manson and co-workers, on the other hand, the energy dissipation mechanisms (massive microcrazing and enhanced matrix yielding) caused by the addition of the rubber particles, resulted in improved crack growth

0022–2461/83 $03.00 + .12 © *1983 Chapman and Hall Ltd.*

resistance in HIPS [8], in rubber modified polyvinylchloride (PVC) [9], and in rubber toughened nylon 6/6 blends [10].

The specific crack tip fracture mechanisms responsible for the improvement in fatigue crack propagation toughness have generally been reconstructed by using *post-mortem* fracture surface topography analysis. However, the toughness derived from the addition of rubber particles relies mainly on increasing energy dissipation by engaging a large volume of material in the deformation process. Therefore, to understand the toughening effect of the rubber particles properly, the total damage zone and, in particular, the nature and size of the energy dissipating crack tip damage processes, should be examined.

With this in mind, the PXE/HIPS/PS system was recognized as an ideal system for the investigation of the fatigue crack advance mechanisms in rubber toughened polymers. Two specific issues were addressed. The role of an elastomeric phase was examined by the addition of rubber to a PXE/PS blend, while the effects of matrix composition were studied by comparison of a rubber toughened PXE/PS blend with a rubber toughened PS system.

2. Materials

Blends of modified PXE/HIPS/PS resins were compounded using a Werner and Pfleiderer 28 mm twin screw extruder, and injection moulded into 10 cm diameter discs (0.32 cm thick). The composition (by wt%) of the various blends used were: 50/0/50, 50/25/25 and 0/25/75 PXE/HIPS/PS, respectively. PXE and PS are completely miscible, hence they form a uniform continuous matrix. The butadiene rubber found in HIPS forms a second phase of rubbery inclusions approximately 0.1 to 1.5 μm in diameter. The amount of rubber was determined by the amount of HIPS (which contains approximately 12 wt% butadiene rubber). The 50/50/50 blend contained no rubber, while the 50/25/25 and 0/25/75 blends contained approximately 3 wt% rubber. The matrix composition was adjusted by altering the relative amount of PXE in the blend. For blends 50/0/50 and 50/25/25 the PXE content was 50 wt% in the matrix, whereas in the 0/25/75 blend no PXE was included. The addition of PXE to the matrix increases the ductility of the blend.

Molecular weight distributions (PXE number average molecular weight, $M_n = 24\,000$, weight average molecular weight, $M_w = 62\,000$; HIPS $M_n = 36\,000$, $M_w = 136\,000$; PS $M_n = 62\,000$, $M_w = 190\,000$) were determined for all starting materials by gel permeation chromatography, using monodispersed polystyrene as a standard reference material.

3. Test methods

Fatigue crack propagation tests were performed using circular compact tension specimens [11]. In all cases, the crack direction was chosen to be along a diameter normal to the gated direction (hence approximately normal to the flow direction) with the starter crack grown from a razor cut by fatigue loading. The stress intensity factor (K_I) for the circular compact tension sample geometry is given by [11]

$$K_I = \frac{F}{BW^{1/2}}(\pi x)^{1/2} Y(x) \quad (1)$$

where

$$Y(x) = \frac{1}{\pi^{1/2}}(30 - 162x + 493x^2 - 664x^3 + 405x^4) \quad (2)$$

and

$$x = a/W \quad (3)$$

for $0.3 < x < 0.7$, where B is the sample thickness, F is the applied load, a is the length of the crack measured from the load line, and W is the width of the sample measured from the load line.

The testing was performed on an Instron 1350 servohydraulic testing machine at a frequency of 10 Hz under sinusoidal loading in tension–tension with a minimum to maximum load ratio of 0.1. Video recordings were made on an NEC VC-9507 time lapse video cassette recorder. The photographic system created an image on a 20 inch monitor with a magnification of 25×, hence increasing the accuracy of crack length measurements during subsequent playback of video recordings.

Subsurface fracture events as well as the damage zone surrounding the crack tip were studied by preparing thinned sections (approximately 50 μm thick for viewing in a transmission optical microscope. These sections were prepared using standard metallographic grinding and polishing techniques and equipment. The subsurface fracture process was also studied by transmission electron microscopy (TEM) using a Hitachi Model 600-3 microscope. All samples were stained in a 10 wt/vol% ($g l^{-1}$) solution of OsO_4 in hexane before microtoming.

The fracture surfaces were examined by scanning

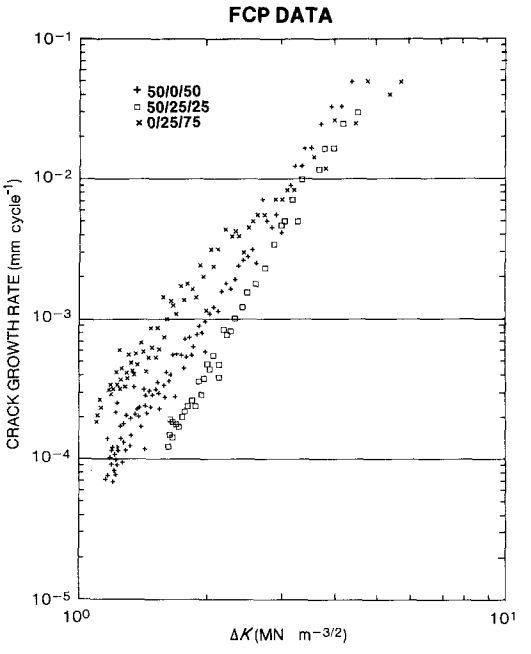

Figure 1 Typical fatigue crack propagation rates for the PXE/HIPS/PS blends.

electron microscopy (SEM) on a Super-II ISI scanning electron microscope. Samples were coated by sputtering with a gold/palladium alloy before observation.

4. Results and discussion

For cyclic loading conditions, the crack growth rate, da/dN, has often been related to the variation in the stress intensity factor by an empirical relationship of the form

$$\frac{da}{dN} = A(\Delta K_I)^m \quad (4)$$

where N is the number of load cycles and A and m are material parameters which are experimentally determined. Although this empirical form (commonly referred to as the Paris–Erdogan relationship) lacks a sound theoretical basis, it has been used to compare the relative FCP behaviour of various polymers [12].

Typical fatigue crack growth data for the PXE/HIPS/PS blends are presented in Fig. 1. In the lower ΔK_I range, there is a reduced crack growth rate with the presence of the rubbery inclusions and with the addition of PXE to PS in the glassy matrix. Without the rubber the 50/0/50 blend shows 2 to 3 times faster crack growth rates compared to the 50/25/25 blend, whereas the 0/25/75 blend propagates 4 to 8 times faster. At higher ΔK_I values, the growth rates of all three blends appear to merge.

These results are in reasonable agreement with those reported by Hertzberg *et al.* [8, 13]. Their HIPS results fall parallel to our results in Fig. 1, but approximately 3 to 4 times faster. Their 10 Hz results for a commercial grade of Noryl™ (which is basically a rubber toughened PXE/PS blend) falls slightly above our 50/0/50 results, whereas their 1 Hz data falls upon our 0/25/75 data, with a slightly greater slope. The differences are most probably due to differences in material composition and other additives used in commercial blend systems.

These FCP results can be qualitatively understood by a detailed examination of the microscopic crack advance mechanisms that occur about the propagating crack tip.

4.1. 50/0/50 PXE/HIPS/PS

A close inspection of individual fatigue cracks in the 50/0/50 blend reveals that each crack is preceded by a large bundle of crazes which are nearly parallel to the crack plane (to within ± 10°). Based on these observations, a likely crack advance mechanism can be postulated. In Fig. 2, an optical micrograph of a thinned section of a fatigue crack, crazes appear to have initiated in the high stress region near the crack tip. As the crack advances through one of the leading crazes, the surrounding crazes propagate forward, gradually diverging away from the crack plane, while additional crazes initiate close to the new crack tip. Thus, a plane normal to the crack growth direction intersects many crazes, with the older crazes intersected further from the crack plane. This craze zone is clearly evident in the cross-sectional view of a thinned section of a fatigue crack in Fig. 3. Similar behaviour has been reported by Kambour and Smith [14], who examined a series of PXE/PS blends in quasi-static plane strain crack propagation tests. During low speed crack growth, a large crazed zone was observed to accompany the propagating crack.

The size of this crazed zone could be approximated using crack tip plastic zone dimensions, which should vary with $(K_I/\sigma_y)^2$ (σ_y is the yield stress) based on a linear elastic fracture mechanics analysis [15]. In Fig. 4 a plot of the craze zone depth against K_I^2 does indeed show a linear dependence.

Although each part of the crack front advances through a single craze, adjacent portions of the

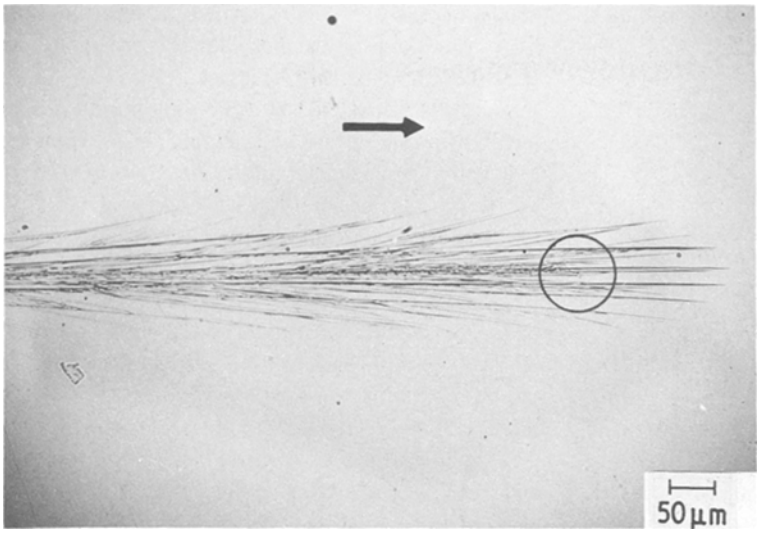

Figure 2 A transmission optical micrograph of a thinned section of an interrupted 50/0/50 fatigue crack, showing the crack tip (circle) preceded by many long crazes. Longitudinal view (section plane containing loading direction and crack growth direction (arrow)). $\Delta K = 1.7\,\mathrm{MN\,m^{-3/2}}$.

propagating crack may advance through different craze planes. The subsequent merger of these adjacent fronts leads to ductile tearing and the formation of so-called "river" lines. These river lines generally extend along the crack propagation direction and are visible on the fracture surface to the unaided eye. A cross-sectional view of one of these river lines can be seen on the fracture surface profile in Fig. 3.

SEM reveals a submicron granular structure which indicates that crack growth indeed proceeds through crazed material.

4.2. 50/25/25 PXE/HIPS/PS

The addition of approximately 3 wt% rubber particles into the matrix produces significant changes in fatigue crack advance mechanisms. The most apparent difference is the visual appearance of stress-whitening in the fracture subsurface zone, which shows up as the darkened region in Fig. 5. No evidence of crazes are visible at this magnification, in sharp contrast to those seen in Fig. 2. A closer inspection of the subsurface region using TEM, however, reveals many microscopic crazes emanating from the rubber particles (Fig. 6). These micron size crazes can be found throughout the darkened region of Fig. 5 and are responsible for the stress-whitening. Similar multiple crazing behaviour has been reported in creep tests on PXE/HIPS blends by Bucknall *et al.* [3] and in uniaxial tension tests on PXE/HIPS/PS blends by Maxwell and Yee [4]. Crazes initiate at the rubber–matrix

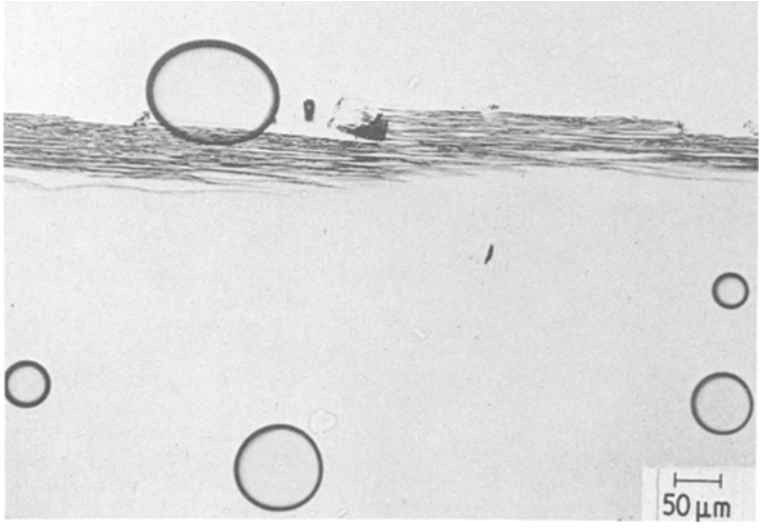

Figure 3 A transmission optical micrograph of a thinned section of a cross-sectional view (plane normal to crack growth direction) of a 50/0/50 fatigue crack showing the multiple craze layers. ($\Delta K \sim 3.0\,\mathrm{MN\,m^{-3/2}}$).

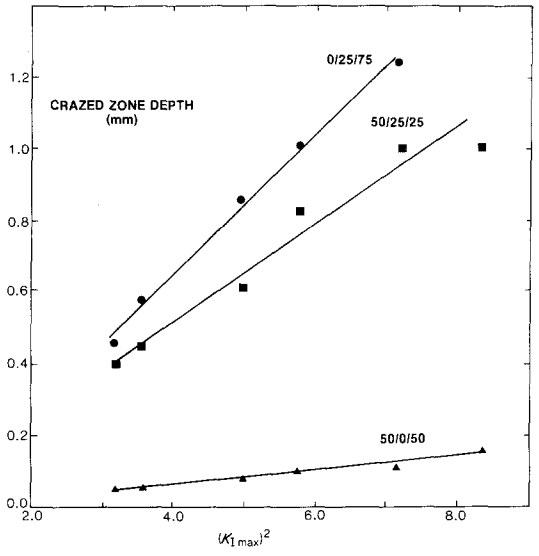

Figure 4 Crazed zone depth against $K^2_{I\,max}$.

interface where stress concentration is greatest and propagate away from the rubber particles. Their growth is believed to be terminated when they interact with other rubber particles or with shear bands initiated from other rubber particles [1] (although no evidence of shear bands was observed in the tests reported here).

As in the case with no rubber particles, the crack advance mechanism is most probably one of crack advance through crazes. The scale of the mechanism, however, is drastically different, reflecting the large differences in craze number density and craze size. In the rubber toughened system, the crack front propagates along adjacent craze planes which merge by a ductile tearing mechanism akin to that which forms the river lines, but on a much more local scale. Thus, on the fatigue fracture surface, granular craze remnants are localized in a halo about the rubber particles (Fig. 7) with ductilely torn material between adjacent craze halos. The fracture surface profile in Fig. 6 clearly reveals the irregular fracture surface topography resulting from the merger of adjacent microcrazes.

In a commercial grade of Noryl^{TM} (which is basically a rubber toughened PXE/PS blend) Rimnac *et al.* [16] observed similar fracture surface topography. They observed rubber particle rupture, strong interfacial adhesion, and multiple craze planes on the fracture surface. They also believed that the rubber particles were the initiation sites of secondary cracks, which left parabolic surface markings (the parabolas mark the loci of intersection of the much faster primary crack as it passes through the secondary crack front). Unfortunately, they were not able to conclude from their observations whether particle rupture initiated the secondary cracks. It is apparent from our studies presented here that craze formation about the rubber particles initiated first, with rubber particle fracture occurring during the actual fracturing process. This is also expected from the high strains necessary to tear the rubber. With good interfacial adhesion, the matrix itself must undergo large strains, i.e. fracture before the rubber particles can rupture.

In Fig. 4, the 50/25/25 blend microcrazed layer depth also shows a linear dependence on K^2_I. There is, however, nearly an order of magnitude increase

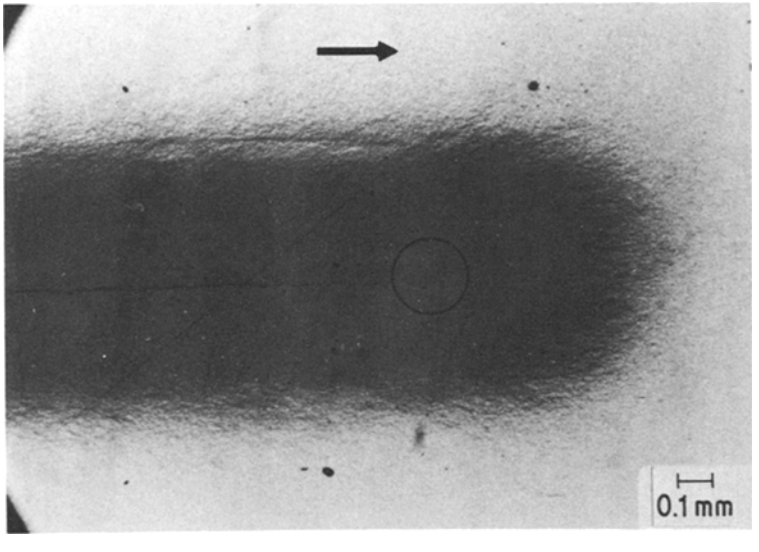

Figure 5 A transmission optical micrograph of a thinned section of an interrupted 50/25/25 fatigue crack. The darkened zone is due to stress-whitening caused by microcrazing. Crack growth direction indicated by arrow, crack tip by circle. (Longitudinal view). $\Delta K = 1.7\,MN\,m^{-3/2}$.

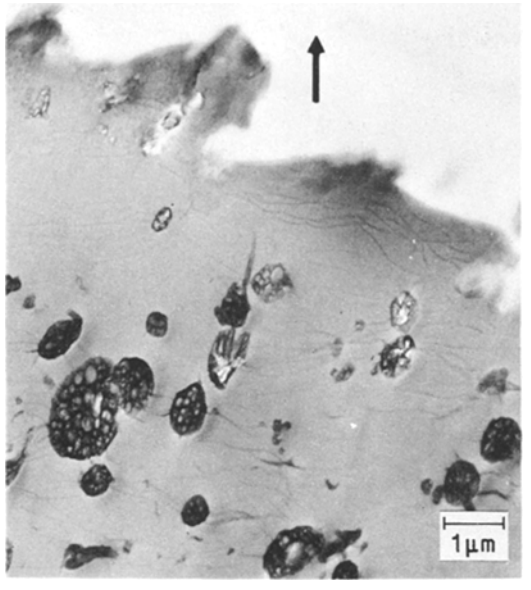

Figure 6 TEM of the subsurface damage zone in the 50/25/25 blend, showing microcrazes initiated at the rubber–matrix interface. The arrow denotes load direction.

in the crack tip crazed zone depth (compared to the 50/0/50 blend). This increase is probably due to the stress concentration caused by the rubber particles and possibly due to the slower crack propagation rates which would provide more time for craze nucleation and growth.

4.3. 0/25/75 PXE/HIPS/PS

With the removal of PXE from the matrix to produce a rubber modified polystyrene, an interesting admixture of crazes and microcrazes accompanies the propagating crack tip. While optical micrographs show large bundles of long crazes (Fig. 8), TEM micrographs of the fracture subsurface reveal many microcrazes emanating from the rubber particles (Fig. 9). These microcrazes appear to grow considerably larger than those observed in the 50/25/25 blend (Fig. 6). The large crazes show considerable variation in length. Most do not appear to have initiated at the crack tip, indicating that they may have resulted from microcrazes initiated far from the crack tip. The crazes diverge from the crack plane with angles larger than those observed in the 50/0/50 blend (Fig. 2) and approach angles of up to $\pm 40^\circ$ from the crack plane. There is also a higher density of crazes in the 0/25/75 blend as compared to the 50/0/50 blend.

The crack tip plastic zones for the three different blends are strikingly different as can be seen by comparing Figs. 2, 5 and 8. These cracks were all grown under the same conditions and were interrupted at the same stress intensity factor range, $\Delta K_I = 1.7\,MN\,m^{-3/2}$. The damage zone extended 0.15 mm ahead of the crack tip for the 50/0/50 blend, 0.65 mm for the 50/25/25 blend and 1.15 mm for the 0/25/75 blend. These values can be compared to the Dugdale plastic zone [17] lengths $(\pi/8)(\Delta K_I/\sigma_y)^2$, of 0.15, 0.25 and 0.56 mm, respectively, where the yield stresses (σ_y) are 90, 69 and 45 $MN\,m^{-2}$, respectively. The larger measured lengths for the two rubber toughened blends are not unexpected since the

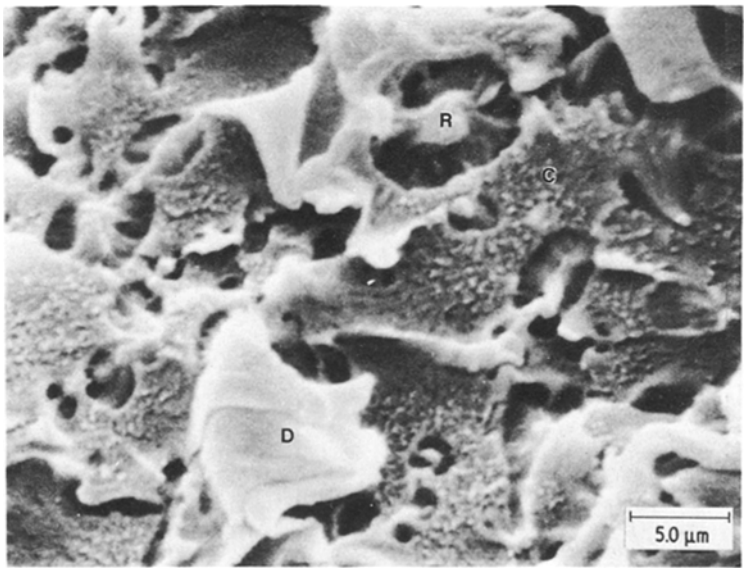

Figure 7 Typical SEM of the fracture surface of the 50/25/25 blend. The rubber particles (R) are surrounded by the granular remnants of a craze (C). Adjacent craze planes are merged by ductile tearing, evidenced by drawn material (D).

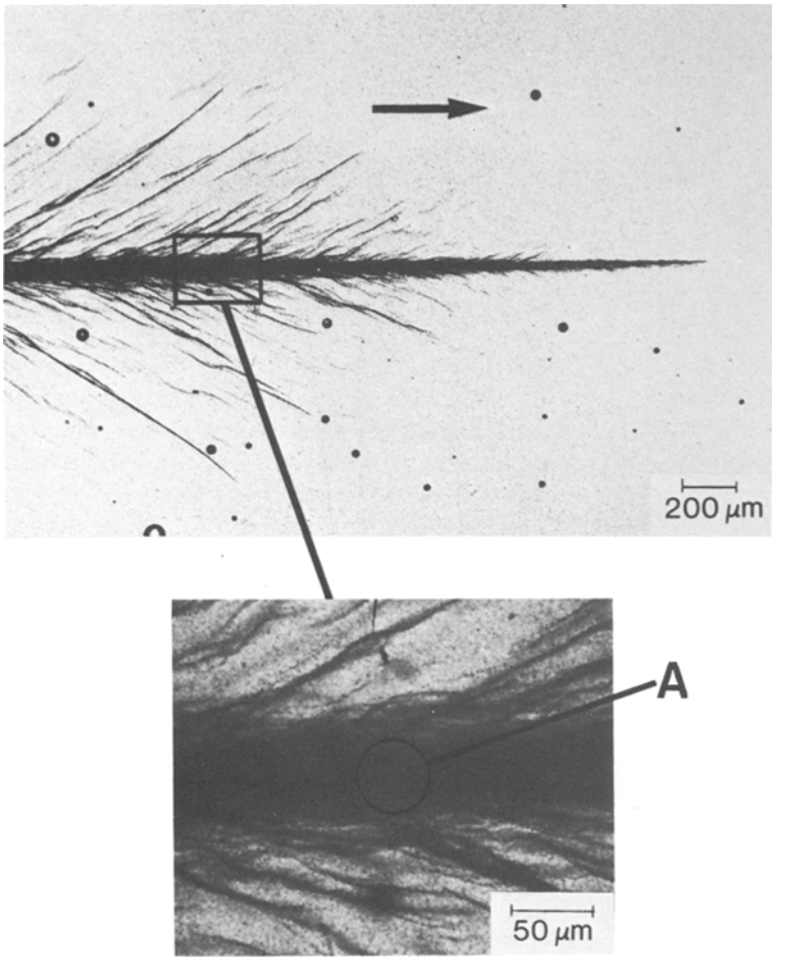

Figure 8 A transmission optical micrograph of a thinned section of an interrupted 0/25/75 fatigue crack showing multiple crazing above and below the fracture surface. The crack growth direction is indicated by the arrow, the crack tip by A. (Longitudinal view). $\Delta K = 1.7\,\mathrm{MN\,m^{-3/2}}$.

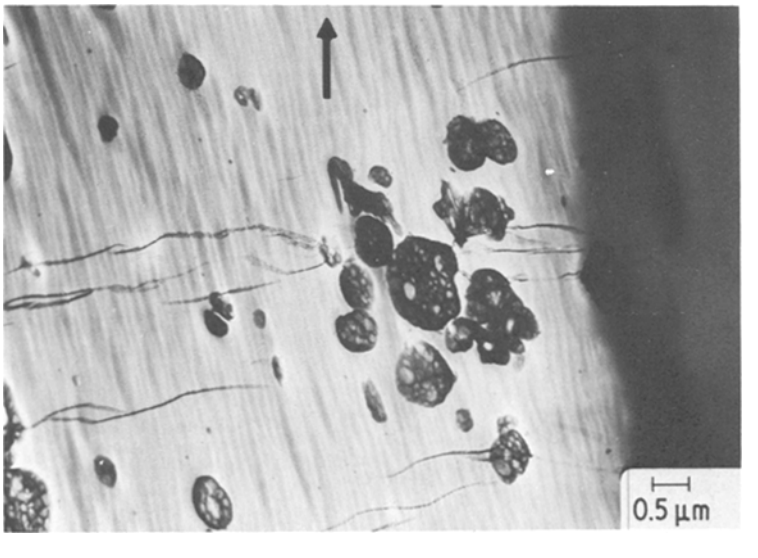

Figure 9 TEM of the subsurface damage zone in the 0/25/75 blend, showing microcrazes initiated at the rubber–matrix interface. The apparent surface on the right-hand side is not the fracture surface, but an artifact of sample preparation. The arrow denotes the load direction.

stress concentrating effects of the rubber particles should extend the craze zone. The different craze divergence angles for the 50/0/50 and the 0/25/75 blends can probably be explained by the overall shape of the damage zone, which reveals the damage development process. For the 50/0/50 blend, the active craze tips appear to be near the forward edge of the damage zone. Lines drawn from the crack tip to each of these active craze tips are nearly parallel to the craze plane. For these craze tips, the maximum principal stress direction is nearly normal to the crack plane. Further craze growth proceeds at 90° to the maximum principal stress direction, assuming a stress bias model [18], and hence craze growth is nearly parallel to the crack plane. In the 0/25/75 blend, however, the damage zone profile is quite peculiar, tapering ahead of the crack tip with a long extended well developed craze region directly ahead in the plane of the crack. The active craze tips are thus not concentrated near the leading edge of the damage zone, but are spread throughout the active damage zone. Lines joining the crack tip with the active craze tips subtend much larger angles with the crack plane (up to 40°). For these craze tips, the maximum principal stress direction points at an angle, to the rear of the crack, thus causing these growing crazes to diverge from the crack plane as seen in the more mature crazes behind the crack tip.

The crazed zone depth also shows a linear dependence on K_I^2 (Fig. 4). As in the case of the 50/25/25 blend, the stress concentration produced by the rubbery inclusions leads to a much deeper crazed zone than for the 50/0/50 blend. The 0/25/75 blend indeed shows the largest crazed zone, which probably reflects the lower crazing stress of PS as compared to an XPE/PS blend.

The fatigue fracture surface also shows granular craze remnants, which is indicative of a multiple crazing mechanism. However, unlike the 50/25/25 blend, the merger of adjacent craze planes does not occur by a ductile tearing process, but results from a more brittle local fracture. The fracture surface found for the 0/25/75 blend is similar to that reported by Manson and Hertzberg [19] in HIPS.

5. Conclusions

There are various energy absorbing crack tip fracture processes associated with the advancing fatigue crack in the PXE/HIPS/PS systems, which affect the FCP behaviour of the various blends. A detailed examination of the fatigue fracture subsurface by transmission optical microscopy and TEM, as well as by SEM has revealed these energy dissipation mechanisms to be:

1. Multiple crazing: many crazes are initiated, either at the rubber–matrix interface or near the crack tip when rubber is not present.

2. An enlarged crazed zone: the stress concentration created by the rubber particles extends the crazed zone considerably beyond the conventional plastic zone for a homogeneous material.

3. Craze growth termination: crazes can be stabilized, i.e. their growth can be limited or terminated by interactions with other rubber particles, or possibly shear bands generated at other rubber particles. Thus, the growth of critically long crazes (which provide an easier path for crack propagation) is prevented and additional microcrazes can be initiated, thereby dissipating more energy.

4. Enhanced shear flow: ductile tearing between adjacent craze planes increases the absorbed energy during the fracture process. Shear flow in the fracture subsurface, although not directly observed in the work reported here, should slow the propagating crack by terminating craze growth, by preventing the initiation of crazes (by offering an alternative deformation process) and by crack tip blunting.

For the 50/0/50 blend, in the absence of an elastomeric phase, several large (macroscopic) crazes form. Although multiple crazing is an energy absorbing process, the presence of large crazes ahead of the crack does not provide much resistance to crack growth. With the addition of rubber particles in the 50/25/25 blend, many short microscopic crazes grow in a much larger crazed zone. All four of the above mentioned energy dissipative mechanisms operate about the propagating fatigue crack and the FCP results reflect this improvement in the fatigue toughness. When the PXE is replaced by PS in the 0/25/75 blend, a large crazed zone is also observed. The PS craze strength, however, is apparently sufficiently low such that craze growth cannot be terminated. Large crazes develop and the FCP rates increase over the 50/25/25 blend.

The increase in FCP resistance due to the addition of rubber particles in PXE/PS is not as dramatic as might have been expected. Similarly, the FCP results for HIPS [8] and for rubber modified PVC [9] (with the exception of the very low M_w PVC) also show definite but not remark-

able improvements. In these three cases, fatigue crack growth rates were at most reduced by a factor of 2 or 3 with the addition of rubber. This modest improvement probably reflects the fact that rubber toughening was historically developed for increasing impact strength and other static properties, rather than fatigue resistance.

A greater degree of rubber toughening optimization was attained in a rubber toughened polycarbonate [20], where the rubber particles produced nearly an order of magnitude decrease in fatigue crack growth rates. The plane strain conditions at the crack tip are believed to be locally relieved by the rubber particles, thereby inducing ductile shear flow in the polycarbonate matrix. This local plane strain relief mechanism has also been reported by Maxwell and Yee [4] in various rubber toughened polycarbonate blends in monotonic tensile tests. Dramatic improvements were also reported in rubber toughened nylon 6/6 [10]. For this case, extensive crack tip heating was observed and the resultant drop in yield stress was believed to cause crack tip blunting. Similar crack tip heating was also observed in non-rubber modified polybutylene terephthalate [21], which produced a distinct thermal transition that changed the damage process from crazing to bulk shear flow. A considerable decrease in crack growth rate was observed during this transition. The role of crack tip heating is being presently investigated and will be reported shortly [21].

In conclusion, although rubber toughened PXE/PS, PS and PVC have shown rather modest FCP improvement, PC and nylon 6/6 have convincingly revealed the magnitude of enhanced FCP toughening that is realizable with the addition of rubber particles. Thus, although the understanding of fatigue toughening mechanisms is still in its infancy, the prospects for further optimization look promising.

Acknowledgements

The authors are indebted to Jim Grande in preparing and photographing the thinned sections, to Ed Koch, Vicki Watkins and Craig Robertson for help with the electron microscopy, and to Roger Kambour, Albert Yee, and Don LeGrand for helpful discussions.

References

1. C. B. BUCKNALL, "Toughened Plastics" (Applied Science Publishers, London, 1977) Chap. 7.
2. A. F. YEE, *J. Mater. Sci.* **12** (1977) 757.
3. C. B. BUCKNALL, D. CLAYTON and W. E. KEAST, *ibid.* **7** (1972) 1443.
4. M. A. MAXWELL and A. F. YEE, *Polym. Eng. Sci.* **21** (1981) 205.
5. J. A. SAUER, M. HABIBULLAH and C. C. CHEN, *J. Appl. Phys.* **52** (1981) 5970.
6. D. WOAN, M. HABIBULLAH and J. A. SAUER, *Polymer* **22** (1981) 699.
7. C. B. BUCKNALL and W. W. STEVENS, *J. Mater. Sci.* **15** (1980) 2950.
8. R. W. HERTZBERG, J. A. MANSON and W. C. WU, "Progress in Flaw Growth and Fracture Toughness Testing", ASTM STP 536 (American Society for Testing of Materials, Philadelphia, 1973) p. 391.
9. M. D. SKIBO, J. A. MANSON, S. M. WEBLER, R. W. HERTZBERG and E. A. COLLINS, "ACS Symposium Series", Vol. 95 (ACS, Washington, DC, 1979) p. 311.
10. R. W. HERTZBERG, M. D. SKIBO and J. A. MANSON, "Fracture Mechanics: Twelfth Conference", ASTM STP 700 (American Society for Testing of Materials, Philadelphia, 1980) p. 49.
11. R. Y. TING and R. L. COTTINGTON, *J. Appl. Polym. Sci.* **25** (1980) 1815.
12. R. W. HERTZBERG and J. A. MANSON, "Fatigue of Engineering Plastics" (Academic Press, New York, 1980) Chap. 3.
13. R. W. HERTZBERG, J. A. MANSON and M. SKIBO, *Polym. Eng. Sci.* **15** (1975) 252.
14. R. P. KAMBOUR and S. A. SMITH, *J. Polym. Sci., Polym. Phys. Ed.* **20** (1982) 2069.
15. J. G. WILLIAMS, "Stress Analysis of Polymers", 2nd edn (J. Wiley and Sons, New York, 1980) p. 332.
16. C. M. RIMNAC, R. W. HERTZBERG and J. A. MANSON, *Polymer* to be published.
17. J. G. WILLIAMS, "Stress Analysis of Polymers", 2nd edn (J. Wiley and Sons, New York, 1980) p. 338.
18. S. S. STERNSTEIN, "Treatise on Materials Science and Technology", Vol. 10, edited by J. M. Schultz (Academic Press, New York, 1977) p. 587.
19. J. A. MANSON and R. W. HERTZBERG, *J. Polym. Sci., Polym. Phys. Ed.* **11** (1973) 2483.
20. To be published.
21. To be published.

Received 15 October
and accepted 23 November 1982